Columnar self-assembly of N,N',N"-trihexylbenzene-1,3,5-tricarboxamides investigated by means of NMR spectroscopy and computational methods in solution and the solid state

Ewa Banach, Christian Invernizzi, Mathieu Baudin, Reinhard Neier, Diego Carnevale

Columnar self-assembly of N,N',N''-trihexylbenzene-1,3,5-tricarboxamides investigated by means of NMR spectroscopy and computational methods in solution and solid state

Ewa Banach,[1] Christian Invernizzi,[1] Mathieu Baudin,[2,3,4] Reinhard Neier[1] and Diego Carnevale[5,*]

[1] *Institut de Chimie, Université de Neuchâtel, Avenue de Bellevaux 51, 2000 Neuchâtel, Switzerland.*

[2] *Institut des sciences et ingénierie chimiques (ISIC), Ecole Polytechnique Fédérale de Lausanne (EPFL), CH-1015 Lausanne, Switzerland.*

[3] *Departement de Chimie, Ecole Normale Superieure, PSL Research University, UPMC Univ Paris 06, CNRS, Laboratoire des Biomolecules (LBM), 24 rue Lhomond, 75005 Paris, France*

[4] *Sorbonne Universites, UPMC Univ Paris 06, Ecole Normale Superieure, CNRS, Laboratoire des Biomolecules (LBM), Paris, France*

[5] *Neuchâtel Platform of Analytical Chemistry (NPAC), Institut de Chimie, Université de Neuchâtel, Avenue de Bellevaux 51, 2000 Neuchâtel, Switzerland.*

Corresponding author: Diego Carnevale

diego.carnevale@unine.ch

Columnar self-assembly of N,N',N''-trihexylbenzene-1,3,5-tricarboxamides investigated
by means of NMR spectroscopy and computational methods in solution and solid state

2

Abstract

The columnar self-assembly resulting from units of *N,N',N''*-trihexylbenzene-1,3,5-tricarboxamide is investigated in solution and solid state by means of NMR spectroscopy. A parallel computational study utilizing both semiempirical and DFT methods allows comparison between experimental results and calculated data for self-assembled and non-assembled structural hypotheses. The hybrid functional B3LYP is compared with the B3LYP-D and B97D functionals to assess contributions due to dispersion interactions. Interatomic distances are studied utilizing ROE experiments on proton spins in solution. Isotropic shifts as measured experimentally are shown to offer a way to assess 'on-the-fly' for self-assemblies. The anisotropic part of the shift interaction for carbon nuclei is probed in the solid state with specific magic-angle spinning experiments. The sensitivity of the NMR parameters for the various carbon environments with respect to the orientation of substituents and packing effects is investigated computationally. We show that all the utilized experimental techniques, in both solution and solid state, and in combination with DFT calculations, are capable of discerning between assembled and non-assembled systems and offer a robust set of independent tools to highlight atomic details in self-organized structures.

Keywords

Introduction

Self-assembly processes are very widely spread in nature and play a key role in most chemical systems relevant to life. The striking feature of these processes relies on the fact that a small number of building blocks can undergo self-organization solely under direction of the intermolecular interaction between the building blocks themselves, and result in very complex macromolecular systems.[1] From the perspective of supramolecular chemistry, this is an invaluable feature as the whole self-assembly process takes place without external intervention. A classic example is given by the DNA double helix, where hydrogen bonds and π-π stacking interactions direct the self-assembling of the base pairs. The elucidation of the interplay between the relatively small number of intermolecular interactions that lead to the creation of ordered superstructures starting from much smaller and simpler units is of fundamental importance to understand chemical recognition processes and hence to be able to design self-assembly systems resulting in materials with desired properties.[2]

Columnar self-assemblies based on benzene-1,3,5-tricarboxamide (BTA) motif result from π-π stacking interactions and formation of maximal number of hydrogen bonds between the individual units.[3-6] These discotic systems[7] are characterized by a helical arrangement of units and have attracted attention as organic electronic elements due to their liquid crystal features.[8] Detailed studies of their aggregation process have highlighted the cooperative nature of these self-assemblies.[9,10] Derivatives of BTA have been investigated as MRI contrast agents,[11] metal complexation agents[12] and utilized in drug-delivery systems.[13] Investigations of BTA-based self-assemblies have focused on the effects of the aliphatic chains,[14,15] introduction of elements of chirality[16] and substitutions on the central aromatic moiety.[17-19] The aggregation process of BTA units and their charge transport properties have been investigated by means of quantum chemical calculations.[20-23] NMR methods based on dipolar interactions and double-quantum approaches have been utilized to characterize structure and dynamics of these systems in the solid state.[24] In spite of all these efforts, and as for most other self-organizing systems, the prediction of the efficiency of the self-assembly

processes related to BTA building blocks is still largely based on empirical data and, hence, remains a challenge.[25]

NMR spectroscopy is an invaluable tool to probe structure and dynamics on the atomic scale for ordered or disordered systems, both in solution or in solid state.[26] The isotropic tumbling that affects molecules in solution allows for high-resolution spectra with typical linewidths of a few Hz. This is due to the fact that only the isotropic part of the interactions is retained by the averaging due to the fast motion, which is typically much faster than the time scale of the NMR experiment. As a result, isotropic peaks are readily identified, with only fine structures due to scalar *J*-coupling left to reveal through-bond interconnectivities between the various chemical environments. Nonetheless, the anisotropic parts of the internal interactions play an important role in relaxation phenomena.

The nuclear Overhauser effect (NOE) is widely used to investigate internuclear distances in molecules in solution.[27,28] This effect relates nuclear spins which are dipolar coupled to one another, i.e., which are in spatial proximity to one another. When a nuclear site within a molecule is perturbed by a radio-frequency (*rf*) irradiation so as to achieve either inversion or saturation of the population difference across the Zeeman eigenstates, a variation in signal intensity is observed for spins which are dipolar coupled to the irradiated one. When compared to the intensity of a pulse-acquire spectrum, this NOE enhancement may be either positive, null or negative, depending on the correlation time of the molecular species in solution. A widely spread modification of this experiment is the rotating frame Overhauser effect (ROE),[29,30] where relaxation and polarization transfer take place in the rotating frame of the *rf* irradiation. The main advantage of this latter technique is that the enhancements are always positive and may be preferred in cases where the NOEs are close to zero. If either NOE or ROE experiments are conducted in the limit of linear growth, measurements of enhancements can be directly related to internuclear distances by means of the relationship:[27]

$$r_{AB} = r_{AX} \left(I_X / I_B \right)^{1/6} ,$$

(1)

Columnar self-assembly of N,N',N''-trihexylbenzene-1,3,5-tricarboxamides investigated
by means of NMR spectroscopy and computational methods in solution and solid state

5

where the index A refers to the irradiated spin, X to a spin whose distance from A, r_{AX}, is known and taken as reference, and B is a third spin whose distance from A, r_{AB}, needs to be evaluated. I_X and I_B are the NOE/ROE enhancements observed for spins X and B, respectively. This is an invaluable tool for structural studies and may supply experimental evidence that allows discharging a structural hypothesis in favor of another. In cases where also *intermolecular* internuclear distances need to be taken into account, such as in dimeric structures, or when equivalent environments supply for more than one interatomic distance, such as for CH_2 groups, an effective distance that takes into account all possible polarization transfer pathways may be utilized:[31,32]

$$r_i^{(eff)} = \left[\left(\frac{1}{r_{i,\,1}^6} + \frac{1}{r_{i,\,2}^6} + ... + \frac{1}{r_{i,\,n}^6} \right)^{-1} \right]^{1/6},$$ (2)

where the i-th spin experiences n polarization transfer pathways with n other spins at distances $r_{i,n}$. These n different pathways are related to direct transfers and indirect effects due to spin diffusion are not considered in this study.[33] An elucidation about the concept of this effective distance $r^{(eff)}$ may be found in Ref. [31].

In contrast to solutions, where the isotropic tumbling motion of molecules averages all interactions to their isotropic components (or to zero if traceless Hamiltonians are involved), in the solid state, the anisotropic part of the internal interactions is retained, and results in broadenings of the NMR lineshapes which are termed inhomogeneous. These result from chemical shift anisotropies (CSA), dipolar couplings, hyperfine couplings with paramagnetic centres and quadrupolar couplings with electric field gradients (EFG).[34] With the exception of 2nd order quadrupolar broadenings, and provided the spinning rate is large enough, the use of magic-angle spinning (MAS)[35,36] allows for an efficient averaging of these inhomogeneities and high-resolution isotropic spectra may be acquired in many cases. Nevertheless, the anisotropic part of the interactions provides very useful information as further means to characterize nuclear environments. Specific techniques have been developed to reintroduce this inhomogeneity in the indirect dimension of 2D experiments.[34] In such a fashion, fast spinning

rates ensure direct acquisition of high-resolution spectra where isotropic shifts may be readily available while the anisotropic interaction is recoupled by the action of the *rf* pulses onto an orthogonal axis. With respect to the anisotropy of the shift interaction, methods have been introduced that are not only capable of recoupling the inhomogeneity averaged out by the fast mechanical rotation, but also amplifying it, as if the experiment was performed at a slower and fictitious spinning rate.[37-42] This allows for more precise measurements of the full shielding tensor than those that one can achieve under static conditions or by spinning the sample at lower rates.[38] With respect to the chemical shift interaction, the following convention of NMR parameters is adopted in this study:[43]

$$\sigma_{iso} = (\sigma_{xx} + \sigma_{yy} + \sigma_{zz})/3 = Tr[\sigma]/3 \qquad (3)$$

$$\Delta_{CS} = \sigma_{zz} - \sigma_{iso} \qquad (4)$$

$$\eta_{CS} = (\sigma_{yy} - \sigma_{xx})/\Delta_{CS} \qquad (5)$$

where the isotropic shift σ_{iso}, the anisotropy Δ_{CS} and asymmetry η_{CS} are expressed in terms of the principal components σ_{xx}, σ_{yy} and σ_{zz} of the shielding tensor σ in its principal axis frame. These principal elements are ordered according to $|\sigma_{zz} - \sigma_{iso}| \geq |\sigma_{xx} - \sigma_{iso}| \geq |\sigma_{yy} - \sigma_{iso}|$. The isotropic chemical shift is given by $\delta_{iso} = \sigma_{ref} - \sigma_{iso}$, where σ_{ref} is a reference shielding.

Density functional theory (DFT)[44] calculations are widely used nowadays as means to interpret and support experimental evidences. In cases where different structural hypotheses are under consideration, DFT calculations can supply the invaluable means to identify the one that agrees best with the experimental data. With respect to NMR spectroscopy, calculations of parameters such as magnetic shielding tensors, EFG tensors or scalar couplings have proven extremely useful in spectral assignment both in solution and solid state.[45-54] Structural details such as internuclear distances or dihedral angles may directly be extracted from the optimized geometries. Most commonly-used density functionals are characterized by a poor description of van der Waals interactions.[55] These long-range attractive contributions play an important role in supramolecular chemistry and self-assembly processes. Therefore, there has been a

considerable effort to develop new functionals capable of describing these dispersion forces.[56]

In this framework, we investigate the columnar self-assembly resulting from BTA in both solution and solid state using a combined approach employing NMR spectroscopy and DFT computational methods. One-dimensional (1D) ^{1}H ROE measurements performed for samples in solution are analyzed in terms of both intramolecular and intermolecular internuclear distances and compared with the values obtained *in silico*. Calculated isotropic shifts allow single 1D ^{1}H NMR spectra to be used 'on-the-fly' as a way to ascertain the presence of a self-assembly in solution. The combination of these two methodologies offer an appealing alternative to multi-sample multi-experiment approaches such as concentration-dependent NMR studies. Furthermore, the anisotropic part of the shift interaction is investigated in the solid state by means of CSA Amplification MAS NMR experiments and the obtained values are compared with those calculated with DFT methods. The possibility to investigate such systems in terms of their chemical shift anisotropy sheds a new light on self-assembly processes and represents a further tool to tackle structural studies of systems capable of self-organization. Computational results produced by the widely-used B3LYP functional are compared with those produced by the B3LYP-D and B97D functionals to highlight structural differences resulting from the inclusion of dispersion forces. The influence of the orientation of the BTA amide functions and π-π stacking effects on chemical shift parameters of carbon sites is considered.

Results and discussion

Solution study

The structure of *N,N',N''*-trihexylbenzene-1,3,5-tricarboxamide (BTA) is shown in Figure 1(a). A central *C₃*-symmetrically substituted aromatic ring (discotic unit) is functionalized by three amide groups containing *n*-hexyl chains. The amide functionalities are linked to the aromatic ring by the carbonyl groups. A simplified scheme depicting a two-unit segment of a columnar self-assembly of BTA is presented in Figure 1(b). The scheme of Figure 1(b) allows the visualization of the main intermolecular interactions that direct the self-assembly process. The

parallel orientation of aromatic rings ensures π–π stacking interactions (highlighted in blue), whereas the three amide groups drive the helical arrangement by forming intermolecular H–bonds with neighboring BTA units (dashed red lines). Figure 2(a) shows a ^{1}H NMR spectrum of a highly-concentrated solution (177 mM) of BTA in CD_2Cl_2 at 9.4 T (400 MHz). By means of the equation $\chi_M = 1/(1+(c/K_D)^p)$ as utilized in concentration-dependent NMR studies of the same BTA assemblies,[19] where c is the total concentration, K_D = 39 mM[19] is the dissociation constant and p = 2.2[19] is a factor that takes into account cooperativity, the molar fraction χ_M of the free monomeric BTA is evaluated to 0.035, thus ensuring that the self-assembled species are predominant in solution and averaging of NMR observables due to fast chemical exchange may be neglected. The NH, CH and NH-C$\underline{H}_2$ resonances, as indicated in the figure, are well resolved and are therefore ideal sites to irradiate in NOE/ROE experiments. Figures 2(b), (c) and (d) show 1D ROE spectra on the same sample of Figure 2(a), where the CH_2 CH and NH resonances are irradiated, respectively. The distortion that affects the CH_2 signal at 1.53 ppm in Figure 2(b) is related to the homonuclear scalar interaction that couples this specific environment with the site that has been irradiated.

In order to interpret these ROE enhancements in terms of internuclear distances, a parallel computational study was performed. A monomeric structure of BTA was firstly optimized with the PM7 semiempirical method as implemented in MOPAC2016.[57] The aliphatic chains of all BTA units were truncated to propyls so as to reduce computational times. This optimized geometry was subsequently used to assemble dimeric, trimeric, tetrameric and pentameric columnar systems. The monomeric and pentameric structures supply a computational model to use for calculations of parameters to be compared with experimental data obtained for either a disassembled or assembled system, respectively. In the pentameric case, only the central unit was considered, with the other two units either up or down the column axis having the sole purpose of smoothing the boundary conditions of the column, i.e., of quenching the perturbations due to the different chemical environments experienced by the 1st and 5th TBA units which terminate the column. In other words, in our computational study,

the central unit of our pentameric assembly is assumed to be representative of a unit of BTA belonging to an infinitely long columnar assembly.

It is important to note at this point that such truncation of a column to a pentameric assembly results in structural parameters such as interplane distances or chemical shifts that are not identical, at equivalent sites, for all units, but rather smear from those of the boundary BTA molecules to those of the central one. This is a consequence of the fact that no periodicity is assumed in our computational study. Again, only the central unit is taken into account in this context as being representative of the columnar assembly as found in either solution or solid state.

All the assembled structures were further optimized at the PM7 level, followed by geometry optimization with DFT methods utilizing the B3LYP functional[58,59] and 6-31G(d,p) basis set. As the B3LYP method does not take into account dispersion forces and more generally long range non-covalent interactions, the DFT optimizations were also repeated with the B3LYP-D and B97D functionals,[60] *ad hoc* parametrized to describe these long-range effects. Figure 3(a), (b) and (c) show the pentameric assemblies optimized with the three considered methods. The columnar arrangement of BTA units with helical pattern of inter-plane hydrogen bonds is particularly evident in the B3LYP case of (a), where an interplane distance of ca. 3.8 Å is found between either the second and third or third and fourth units. In the cases of B3LYP-D and B97D, instead, a more compact pentamer is obtained, with π-π stacking distances between the same units of ca. 3.2 Å in both cases. This is in agreement with previous observations reported in the literature.[61] It is worth mentioning in this context that X-ray diffraction data related to previous studies on *N,N',N''*-tris(2-methoxyethyl)benzene-1,3,5-tricarboxamide revealed an interplane distance in the column self-assembly of 3.62 Å.[19] Furthermore, as can be seen in (d), (e) and (f), from views down the column axis of the same structures of (a), (b) and (c), respectively, the alignment of the benzene moieties in the B3LYP case is more regular, with BTA units experiencing a progressive average twist of 58.6 ± 1.0° around the column axis as one moves from plane to plane down the columnar assembly. This arrangement of units is directed by the establishment of the hydrogen-bonding network and results in the helical nature of the

column. A measure of this twist may be given by the average <u>H</u>-<u>C</u>-<u>C</u>-<u>H</u> and O=<u>C</u>-<u>C</u>-<u>C</u>-<u>C</u>=O interplane dihedral angles given in Table 1, with the first two sites defining each dihedral angle belonging to the nth unit of the column and the second two to the nth+1 unit. In the cases of B3LYP-D and B97D of Figure 3(e) and (f), in contrast, the progressive average twist of BTA units across the different planes of the columnar assembly, as dictated by the H-bonding network and by π-π stacking interactions, is 62.8 ± 2.0 and 62.7 ± 2.4°, respectively, thus resulting in a less regular alignment of benzene moieties, as viewed down the column axis.

The orientation of the amide functions within the self-assembly may be measured by the dihedral angles H-<u>C</u>-<u>C</u>-<u>C</u>=<u>O</u> as given in Table 2. The structure produced by the B3LYP functional results in amide functions oriented so that this average angle amounts to θ = −34.4 ± 3.6° whereas the B3LYP-D and B97D functionals result in amide functions closer to coplanarity with the benzene cores, with average dihedral angle amounting to −28.6 ± 6.0 and −25.9 ± 11.4°. These values reflect the more compact structure obtained when dispersion interactions are taken into account. In this latter case, the larger standard deviation of values confirms the less regular alignment of BTA units obtained with the B3LYP-D and B97D functionals.

Furthermore, one of the amide functions of the boundary BTA unit terminating the column structure (5th unit in Table 2) produced by the B97D method is oriented discordantly from the other two within the same unit, with H-<u>C</u>-<u>C</u>-<u>C</u>=<u>O</u> dihedral angles amounting to θ = − 17.9, −15.5 and +9.6°. This feature can be easily seen in the electron density isosurfaces color-coded with the electrostatic potential given in Figure ESI1 and represents possible different chemical environments, or structural irregularities, at the boundaries of the assemblies. In contrast, the more regular structure produced by B3LYP results in concordant angles of θ = − 29.5, −29.7 and −29.3° for the same unit.

By inspection of the dihedral angles H-<u>C</u>-<u>C</u>-<u>C</u>=<u>O</u> given in Table 2, when moving from either the 1st or the 5th terminal BTA units towards the central 3rd one, one can generally see a progressive adjustment of this structural parameter, with progressively smaller standard deviation of values. This observation indicates that our choice of a pentameric system is

effective in 'quenching' the propagation of structural irregularities from the boundaries of the self-assembly up to the considered central unit.

The DFT-optimized monomeric and pentameric structures thus produced were utilized to measure proton-proton interatomic distances. These values were compared with those derived from the experimental ROE measurements of Figures 2. The effective distance of Eq. (2) was utilized so as to take into account for the larger number of polarization transfer pathways only possible in the assembled systems, i.e., for both intra and intermolecular proton-proton interatomic distances. Figure 4 shows the differences between interatomic distances $\Delta r = \left| r_{ROE} - r_{DFT} \right|$ as histogram. The larger these values, the larger the disagreement between the computational model and the experimental measurement. Figure 4(a) (b) and (c), show data related to the three DFT methods utilized in this study, i.e., B3LYP, B3LYP-D and B97D, respectively. All results related to the three experiments with irradiations on the NH, CH and CH_2 are shown. In these histograms, data shown in blue and red refer to the monomeric and pentameric DFT structures, respectively. With the only exception of the NH experiment as interpreted by the B3LYP method (highlighted by a dashed rectangle), all other cases show that smaller mismatches between the computed model structure and the experimental measurements are obtained when the pentameric structure is considered. In other words, our ROE measurements indicate the BTA as assembled in our sample. The data of Figure 4 shows that, in the case at hand, and when an appropriate model and functional are assumed, our combined NMR-DFT approach produces errors in the measurement of internuclear distances which are generally smaller than 0.4 Å. Considering the good performance and agreement between B3LYP-D and B97D functionals, the discrepancy obtained for the NH case when the B3LYP method is employed can be rationalized considering an overall overestimation of interplane distances due to lack of description for dispersion forces. With this respect, it is worth bearing in mind that the larger H-<u>C</u>-<u>C</u>-<u>C</u>=<u>O</u> dihedral angles (Table 2) produced by B3LYP – related to a structural 'expansion' of the column – result in the increase in the intramolecular internuclear distance between the NH and the CH proton sites.[62]

These results indicate that (i) ROE experiments can be used to ascertain whether BTA units in solution have undergone self-assembling or not and (ii) the use of DFT methods that take into account for the effect of non-covalent dispersive interactions is required when interatomic distances in such supramolecular self-assemblies are considered.

In the attempt to obtain ROE measurements related to a non-assembled BTA monomeric state, a more dilute 5 mM solution of BTA in acetone-d_6 was considered. At this concentration, the predominant species in CD_2Cl_2 is the isolated monomeric BTA, for which $\chi_M = 0.989$.[19] Our choice for acetone, a H-bond acceptor solvent more polar than CD_2Cl_2, has the purpose of further destabilizing any assembly in favor of the monomer by disrupting the interplane H-bonding network. The corresponding ROE spectra are shown in Figure ESI2. The diluted sample results in much larger error bars in the $\Delta r = \left| r_{ROE} - r_{DFT} \right|$ profile that prevent the identification of a preferred structure (Figure ESI3). It is worth noting that the order of CH and NH resonances at this concentration is inverted. This observation has been confirmed by ^{1}H-^{13}C HSQC spectra (Figure ESI4). The overall inaccuracy of the ROE measurements in the more diluted case may be reasonably ascribed to i) much lower S/N, ii) much longer spin locking pulse (50 ms vs 5 ms used for the 177 mM sample) in the attempt to gain sensitivity. This latter feature results in a less strict fulfillment of the condition of linear growth of the ROE enhancement. Finally, iii) chemical exchange of the NH protons with the residual water of the solvent – more likely to be relevant when BTA is not assembled – introduces leakage of the ROE enhancement towards the water proton bath.

The DFT-optimized BTA structures for monomer, dimer, trimer, tetramer and pentamer have subsequently been used to calculate the chemical shifts for the proton and carbon nuclei at the B3LYP/6-31+G(d,p) level of theory, i.e., with addition of diffuse functions on heavy atoms with respect to the geometry optimizations. In the case of trimers and pentamers, only the central units were considered, for dimeric structures both units were averaged, whereas for the tetramers the two central units were averaged. Within a given unit, all 'equivalent' sites were also averaged. In other words, say, three C̲=O shifts were averaged to one single shift, three C̲H$_2$ shifts were averaged to one single C̲H$_2$ environment, and so on so forth. Figure 5(a), (b) and (c)

show the chemical shifts for the three considered environments, CH, NH and CH_2, as calculated with the B3LYP, B3LYP-D and B97D functionals, respectively. It is interesting to notice that the NH and CH resonances have opposite trends as one moves from the monomeric structure to an assembled one. This is in agreement with the behavior experimentally observed in the concentration-dependent NMR study of BTA.[19] The crossing of isotropic shift for these two environments is correctly predicted by all considered methods. The B3LYP calculations of Figure 5(a) were repeated with inclusion of solvent effects. The corresponding plot, shown in Figure ESI5, indicates that only the NH resonance is affected, with a systematic average deshielding of 0.68 ppm, from the monomer to the pentamer. The inversion trend observed for the CH and NH resonances is conserved when solvent effects are taken into account. More importantly, no particular change is observed on the structures, with the same regularity of stacking of BTA units as shown of Figure 3(a) and (d), and with interplane distances for the pentamer of ca. 3.7 Å, i.e., very similar to those obtained by the same functional without inclusion of solvent effects (Cartesian coordinates are given in ESI).

The diluted (5 mM) and concentrated (177 mM) samples considered in this study allow us to readily obtain proton chemical shift from simple 1D spectra for solutions where monomeric and assembled structures, respectively, are predominant. These experimental chemical shifts can then be correlated with those calculated with DFT methods for a monomeric and a pentameric structure, with the central unit of this latter being representative of the environment experienced by a BTA unit when in aggregated state. The corresponding results are shown in Figure 5(d), (e) and (f), for the B3LYP, B3LYP-D and B97D methods, respectively. The terminal CH_3 groups of the aliphatic chains were also included in these plots. One can readily appreciate that the experimental shift obtained from the diluted sample (empty data points in Figure 5(d-f)) correlate very well with those calculated for the monomeric structure, with R^2 = 0.987, 0.987 and 0.994, for B3LYP, B3LYP-D and B97D, respectively. If the same experimental shifts are correlated with those calculated for the pentameric assembly, the correlation factors become R^2 = 0.820, 0.816 and 0.824. In this latter case, the data points related to the CH and NH resonances are significantly brought away from the ideal correlation. These displacements of

data points are highlighted by empty arrows in Figure 5(d-f). Analogously, the experimental shifts from the concentrated sample correlate very well with those calculated for the pentameric structure, with R^2 = 0.999, 0.997 and 0.999, for B3LYP, B3LYP-D and B97D, respectively. When the same shifts are correlated with those calculated for an isolated monomer, the correlation coefficients drop to R^2 = 0.758, 0.759 and 0.784. As previously discussed, the NH and CH data points are significantly displaced away from the ideal correlation (black arrows). Therefore, the NH and CH environment appear to be very sensitive to assembling processes in terms of their chemical shifts. The plots of Figure 5(d-f) also reveal that, for this particular chemical system, B3LYP, B3LYP-D and B97D functionals are all adequate in discerning between assembled and non-assembled structures in terms of isotropic chemical shift values of the proton sites involved in the self-assembly.

Solid-state study

MAS NMR techniques offer an invaluable tool in investigations of structure and dynamics of self-assemblies in the solid state.[63-66] In most cases, double-quantum techniques based on dipolar couplings between high-abundant proton spins were exploited. Carbon chemical shifts have been investigated both experimentally and computationally in columnar phases of 2,3,6,7,10,11-hexahexylthiotriphenylene.[67,68] In this study, we probe the chemical shift anisotropy of carbon sites as a means to extract experimental evidence of columnar self-assemblies in a powdered sample of BTA. The ^{13}C Cross-Polarization (CP) MAS spectrum of a powder of the BTA considered in this study is shown in Figure 6(a). The chosen spinning frequency of v_{rot} = 20 kHz (200 ppm at 9.4 T) allows for a high-resolution spectrum, with all spinning sidebands being of negligible intensity and laying outside of the spectral window. Folding or aliasing is prevented by the use of digital filters. The two resonances at 168.8 and 136.4 ppm, ascribed to the carbonyl (C=O) and aromatic quaternary (C) carbon sites, respectively, appear as well resolved single environments, with a FWHM of ca. 100 Hz, as indicated by black arrows. In contrast, the aromatic CH resonance at 126.2 ppm results from the overlap of at least three different peaks. Therefore, the CH resonance reveals a degree of inhomogeneity in terms of chemical environment for this carbon site in our BTA in the solid

state. In contrast with the aliphatic peaks appearing in the 0 – 50 ppm range, the C=O, C and CH environments are expected to be characterized by a substantial chemical shift anisotropy. In fact, as shown in the ^{13}C CP MAS spectrum of Figure 6(b), a series of spinning sidebands related to these three sites is readily highlighted as the spinning rate is decreased to v_{rot} = 5 kHz. It is worth noting that the shoulders appearing on both sides of the CH resonance at 126.2 ppm in both spectra of 6(a) and (b), can also be highlighted on all spinning sidebands associated with this environment. This indicates that similar anisotropies characterize these CH environments. Figure 6(c) shows a fit of the spectrum in (b) assuming one single site for the C=O resonance, one single site for the C resonance and three sites for the CH resonance, so as to take into account for the shoulders of this peak. The aliphatic region was excluded from the fitting procedure. Nonetheless, the resulting fit is substantially in good agreement with the experimental spectrum, and produces the anisotropic parameters summarized in Table 3. Figure 6(d) shows a dipolar-dephasing spectrum which confirms the assignment of the CH resonance at 126.2 ppm as this peak disappears when allowed to diphase under dipolar interactions with its neighboring proton. The disappearance of this peak and of all its spinning sideband family is indicated in figure by a dashed arrow. Importantly, the CP spectra of (a) and (b), along with the simulation of (c), indicate that, as the spinning rate is decreased, spinning sidebands at lower frequency appear in the aliphatic region thus resulting overlapped with the other isotropic aliphatic peaks. This condition prevented the fitting procedure used in Fig. 6(c) to take into account for these lower-frequency spinning sidebands.

An ideal condition would be one where the spinning rate is large enough so as to ensure isotropic peaks to be readily determined and avoid overlaps of resonances or spinning sidebands, but at the same time not large enough so as to result in an adequate number of spinning sidebands for analysis purposes. In order to achieve these advantages and obtain a more reliable characterization of the shielding tensors associated with these three carbon environments, a two-dimensional approach was chosen. The ^{13}C CP CSA Amplification[39,40] spectrum of the BTA considered in this study is shown in Figure 7(a). The F_2 projection results in the conventional ^{13}C CP spectrum recorded at the true spinning rate of 20 kHz. This projection is

analogous to the spectrum of Figure 6(a). The F_1 projection instead results in a pure shift CSA amplified dimension. The amplification factor was 8. Therefore, the series of data points that construct the F_1 projection of the 2D spectrum represents the intensities of a spinning sideband pattern as if the experiment was performed at a fictitious spinning rate of 20/8 = 2.5 kHz. The CSA patterns related to the individual sites of interest may be readily extracted from the 2D spectrum, as indicated by the dashed lines and arrows, and are shown in (b), (c) and (d). The corresponding fits are overlaid in red. It is worth bearing in mind that the experiment is designed so that the anisotropic part of the shift interaction is amplified whereas the isotropic part is refocused. This feature results in the projections of (b-d) to appear as if they all were associated with sites with δ_{iso} = 0 Hz. This has the advantage of reducing the space of variables that needs to be explored by the fitting procedure, as the only parameters that need to be considered are Δ_{CS} and η_{CS}. These fits are also considerably faster than those of Figure 7(c) as only a number of points that matches the indirect dimension increments need to be simulated, provided *in-silico* observation is performed stroboscopically with the rotor period. In our case, only 32 points needed to be simulated. Moreover, and in contrast with the fit shown in Fig. 6(c), only one site needs to be included in each fitting procedure as the indirect dimension of the 2D data set allows extraction of single-site CSA patterns. Furthermore, there is no need to simulate the full multi-pulse 2D experiment as a simple pulse-acquire experiment at the fictitious spinning rate suffices. The quality of the fits presented in Figure 7(b-d) is remarkably good. An estimation of the errors associated with these measurements of the Δ_{CS} and η_{CS} parameters for each analyzed carbon environment is given by the 95% confidence interval as extracted from the *rms* deviation 2D contour plots shown in (e-g).[41,42,69] The parameters extracted at the minima of these 2D surfaces are given in Table 3 for the three sites of interest.

The CSA Amplification 2D experiment of Figure 7 allowed for a full characterization of the chemical shift interaction, both in its isotropic and anisotropic components. These parameters shed a light on the solid-state BTA system with an atomic-scale resolution and could be used to investigate different structural hypotheses. In our context, we could ascertain whether these MAS NMR measurements are consistent with the existence of columnar self-

assemblies in the solid state. As test-bed of our analysis, the hypothesis of a non-assembled system has also been considered. DFT calculations of the NMR parameters performed on the pentameric structures shown in Figure 3 supply a set of parameters that can be related to a columnar self-assembly of BTA units. In order to obtain an analogous set of parameters that instead refers to a non-assembled system, the computational approach shown in Figure ESI6 was adopted. Six BTA units were arbitrarily arranged as faces of a cube with edge length of ca. 14.5 Å. This configuration of molecules is shown in Figure ESI6(a). A schematic representation of the cubic arrangement is also depicted in (b). This initial configuration of BTA units has no physical meaning but rather serves as an arbitrary starting point for a geometry optimization procedure that prevents the units to self-assemble in a columnar superstructure. This system was subsequently allowed to relax by means of a geometry optimization performed at the PM7 semiempirical level. The resulting superstructure was then further refined with DFT methods utilizing the three considered functionals and 6-31G(d,p) basis set. These hexameric arrangements obtained with B3LYP and B97D are shown in Figure ESI6(c) and (d), respectively. As expected, this procedure produces structures that do not show any columnar arrangement of BTA units and that are meant to mimic a non-assembled system. Both structures were subsequently used for the calculations of the chemical shift parameters. Only the innermost molecule of both arrangements was considered. This molecule is shown in black in Figure ESI6(c) and (d). The corresponding NMR parameters are assumed to be representative of a disordered system in the solid state.

Figures 8(a-c) show the correlations between the CSA parameters measured experimentally with our MAS techniques and those calculated for the structural hypotheses considered in this study, i.e., the columnar pentameric assembly of Fig. 3 and the collapsed cubic arrangement of Fig. ESI3, for B3LYP, B3LYP-D and B97D functionals. As previously discussed, in the case of the columnar pentameric assembly, only the central BTA unit was considered whereas, in the case of non-assembled hexamer of Figure ESI6, only the innermost BTA unit was taken into account. Computational data related to the monomeric BTA is also included for sake of comparison. The error bars on the experimental axes are given in Table 3.

Also the anisotropy of the aliphatic CH_2 carbon sites is included in these plots. The ideal 1:1 correlation is indicated by a dashed line. Figure 8(d) shows the correlation coefficients R^2 related to the plots of (a-c), as histogram. Light blue, dark blue and red data refer to the CSA parameter as calculated with B3LYP, B3LYP-D and B97D, respectively. All methods show that the monomeric case results in the lowest qualities of correlation (R^2 = 0.971, 0.984 and 0.975, respectively). This is not surprising as this structural model is meant to represent a BTA unit in solution (or vacuum). More interestingly, our experimentally measured anisotropies correlate slightly better with those calculated on the self-assembled pentameric structure than with those resulting from the non-assembled arrangement of BTA units of Fig. ESI6. Differences in qualities of correlation are found on the third decimal place, with the B3LYP method yielding R^2 = 0.997 and 0.999, B3LYP-D giving R^2 = 0.993 and 0.995, and with B97D method resulting in R^2 = 0.994 and 0.996, for the non-assembled and assembled case, respectively. Data referring to the qualities of correlation for the isotropic shift are shown in grey scale in the histogram of Figure 8(d). In contrast with the shift anisotropy Δ_{cs}, the isotropic part of the shift interaction δ_{iso} seems to be, in this particular case, considerably less informative, with very similar R^2 coefficients for all the structural hypotheses considered.

As previously stated, averaging of both isotropic and anisotropic chemical shifts on 'chemically-equivalent' sites was performed on the selected units of BTA in the calculated structures considered in this study. Within this *modus operandi*, we have shown that measurements of CSA parameters can be used to probe structural details in columnar self-assemblies of BTA in the solid state. In contrast, isotropic shifts do not supply with the required sensitivity to discriminate between different structural hypotheses in these particular systems. However, further insights may be discerned by considering the distribution of isotropic shifts within the selected units of BTA in our structural models when those are not subject to averaging over equivalent sites. This is particularly useful for solid samples where crystal-packing effects, or more generally, as in our case, intermolecular interactions can lift the degeneracy of chemical sites in terms of magnetic shielding. Figure 9 shows a series of simulated ^{13}C spectra which assume *all* the calculated isotropic shifts (i.e., for the 12 carbon

sites without averaging related to three C=O, three C, three CH and three CH_2) associated with the selected units of BTA within our structural models. The resulting spectra for the monomeric, pentameric assembly and non-assembled (collapsed cubic arrangement) structures are shown in 9(a), (b) and (c), respectively. Only the computational data produced by the B3LYP method is shown for simplicity. A line broadening of 100 Hz was applied to each Lorentzian function utilized to reconstruct the spectra. This line broadening is similar to that experimentally observed in the MAS 1D spectra of Figure 6. Analogously to the correlations of Figure 5 and 8, also the aliphatic CH_2 environments have been included in these spectra. In (a), the main four environments can be readily identified, with subtle 'splittings' of ca. 115 Hz observed on the C and CH_2 peaks. These 'splittings' represent chemical inequivalences at these sites produced by the geometry optimization procedure. These inequivalences are related to the fact that, in the optimized structure of a monomeric BTA system, two carbonyl groups are pointing up and one is pointing down, with H-<u>C</u>-<u>C</u>-<u>C</u>=<u>O</u> dihedral angles of 14.8, 15.3 and −17.3° for B3LYP and 17.7, 16.1 and −19.4° for B97D. This results in small variations in chemical shifts at the C and CH_2 sites. In a real system in solution, free and fast rotation of the substituents about the <u>C</u>-<u>C</u>=O bonds will result in averaged environments (i.e., single peaks) as perceived on the NMR time scale. This feature legitimates the common procedure of averaging the calculated chemicals shifts for chemically-equivalent environments when solution data is analyzed. Figure 9(b) shows the ^{13}C NMR spectrum resulting from all 12 environments of the central BTA unit of the pentameric self-assembly of Fig. 3. It is interesting to notice that the degree of chemical shift dispersion in the columnar self-assembly is substantially identical to that calculated for the isolated monomeric unit of (a). Tiny splittings of ca. 100 Hz are observed on the C=O and aromatic CH resonances. However, these splittings are comparable with the inhomogeneous linewidth observed experimentally in the spectra of Figure 6(a, b) and therefore justify the averaging of the calculated chemical shifts for the self-assembly as performed in this study. In other words, the chemical shift inequivalences calculated by DFT methods for carbon nuclei in a columnar self-assembly of BTA units are not predicted, as is indeed the case with the only exception of the CH resonance at 126.2 ppm, to be observable in the experimental spectra of Figure 6. When considering instead the distribution of chemical shifts observed in (c), resulting from the non-

assembled structure of Fig. ESI3, we find a substantially larger differentiation in terms of chemical environments, with spreads of chemical shift of ca. 280 Hz, i.e., about three times larger than the inhomogeneous linewidth experimentally observed in the experimental spectra of Fig. 6. Therefore, and in agreement with the analysis performed on the CSA parameter, by considering the spread of the isotropic part of the shift interaction as calculated for the different structural hypotheses considered in this study, a clear evidence of consistency of the experimental solid-state results with the hypothesis of a columnar self-assembled structure can be found.

A further series of calculations was performed in order to highlight the effects on the NMR parameters of i) different truncations of the aliphatic chains, ii) the orientation of the amide functions with respect to the aromatic core and iii) non-covalent and dispersive contributions. The corresponding results are shown in Figure ESI7 and 8. A brief discussion on this data set is also given in the ESI. The results indicate that the carbon site most affected by variations of the HCCCO dihedral angle and by the 'loosing' of π-π stacking effects is the CH of the aromatic core, with the other carbon sites C and CO experiencing smaller effects. In contrast, very little effect on all considered carbons is produced by variations of the length of the aliphatic chain.

Conclusions

The columnar self-assembly of *N,N',N''*-trihexylbenzene-1,3,5-tricarboxamide (BTA) units has been investigated in both solution and solid state by means of NMR techniques. A parallel computational study that combined semiempirical and DFT methods has been performed to produce structural parameters to be compared with those measured experimentally, namely, interatomic distances for ROE solution measurements, isotropic chemical shifts to be compared with those obtained from simple 1D solution spectra and anisotropic shifts to be compared with those measured with specifically designed multi-pulse MAS methods in the solid state. We show how a combination of NMR and computational methods allows to shed a light on self-assembly processes in solution by means of simple 1D measurements without the need to follow the assembling process in a multi-sample multi-experiment approach such as

that of concentration-dependent NMR studies. More specifically, the analysis of ROE enhancements that take into account both intra and intermolecular interatomic distances allows to ascertain the presence of BTA self-assemblies in solution. DTF methods that include description for non-covalent dispersive interactions are required for such purpose. We also show that both isotropic and anisotropic parts of the shift interaction can be used to characterize BTA-based columnar assemblies in the solid state. With respect to both isotropic and anisotropic chemical shift parameters, the computational analysis of i) the influence of the orientation of the amide functions and ii) effects of dispersive forces, indicates that the CH is the most sensitive carbon environment to monitor columnar self-assembling processes of BTA units.

Experimental and computational details

All solution spectra were acquired in Neuchâtel, at the Neuchâtel Platform of Analytical Chemistry (NPAC), on a Bruker Avance-II spectrometer equipped with a 5 mm narrow-bore magnet operating at 9.4 T (400 MHz for ^{1}H). All conventional NMR experiments were performed at room temperature, with typical recovery delays of d_1 = 2 s and 90° pulse lengths of τ_p = 9.6 μs corresponding to an *rf* field strength of ν_1 = 26 kHz. The 1D ROESY spectra of Figures 2 and 3 employed spin locking with an *rf*-filed strength ν_1 = 3 kHz and length τ_{SL} = 5 and 50 ms, respectively, and sinc-shaped selective π pulses of length τ_p = 10 ms.

All ^{13}C CP MAS spectra of Figure 7 were recorded in Sion, at the Ecole Polytechnique Fédérale de Lausanne (EPFL), on a wide-bore Bruker 400 spectrometer (9.4 T) with an Avance-III console, using 2.5 mm ZrO$_2$ rotors and a triple-resonance MAS probe. The *rf*-field amplitude for proton and carbon hard pulses was ν_1 = 132 and 109 kHz, respectively, corresponding to 90° flip-angle pulse lengths of τ_p = 1.9 and 2.3 μs, respectively. A recycling delay of d_1 = 2 s was used in all cases, with a spinning rates of ν_{rot} = 20 and 5 kHz. The *rf*-field strength for the cross-polarization step was ν_1 = 70 and 50 kHz for ^{1}H and ^{13}C, respectively with a contact time τ_{CT} = 3.5 ms. The amplitude of the ^{1}H pulse was ramped from 90 to 100% during CP. The spectra were referenced to TMS using adamantane as external reference. The amplification factor of the CSA

Amplification experiment of Figure 7 was 8, corresponding to a spinning sideband pattern of a fictitious MAS rate of 20/8 = 2.5 kHz mimicked in the indirect dimension, and 576 transients were averaged for each of 32 t_1 increments.

The structures of BTA in its monomeric and *n*-meric (*n* = 2, 3, 4 and 5) forms were preliminarily optimized with the PM7 semiempirical method as implemented in MOPAC2016.[57] A further optimization was performed with DFT methods utilizing B3LYP, [58,59] B3LYP-D and B97D functionals,[60,71] with the 6-31G(d,p) basis set, as implemented in Gaussian09 Revision A.01.[70] The keyword IOp(3/124=3) was used to include empirical dispersion correction for the B3LYP functional. The influence of solvent effects was investigated utilizing the PCM method.[72] The convergence criteria for the DFT optimizations required variations of energy between two successive iterations to be smaller than 3×10^{-2} kJ/mol. Frequency calculations were subsequently run at the same level of theory to exclude imaginary vibrational modes. The structures thus obtained were used to calculate the magnetic shielding tensors of both ^{1}H and ^{13}C nuclei with the GIAO method[73,74] with all functionals, and 6-31+G(d,p) basis set. All chemical shifts were referenced to those of TMS at the corresponding level of theory. The shielding tensors σ as calculated by Gaussian09 are expressed in an arbitrary molecular frame. The principal elements σ_{xx}, σ_{yy} and σ_{zz} where obtained by diagonalization of σ according to $\sigma^{(D)} = P^{-1}\sigma P$, where $\sigma^{(D)}$ is the diagonal matrix with the eigenvalues of σ as elements and P is the matrix constituted by the eigenvectors of σ as columns. A scheme depicting the computational procedure followed in this study is shown in Figure 10. In order to reduce the computational time required for the DFT steps of the scheme, the aliphatic chains of BTA were truncated to propyls. DFT calculations were performed at the EPFL on a Ubuntu Linux 12.04 workstation equipped with 16 2.27 GHz CPUs and 24 GB of RAM.

Acknowledgements

References

[1] J. W. Steed, J. L. Atwood and P. A. Gale, in *Supramolecular Chemistry: From Molecules to Nanomaterials*, ed. P. A. Gale and J. W. Steed, John Wiley & Sons Ltd., Chichester, UK, 2012, vol. 1, pp. 3–7.

[2] D. Philp and J. F. Stoddart, *Angew. Chem. Int. Ed. Engl*. 1996, 35, 1154.

[3] S. Cantekin, T. F. A. de Greef and A. R. A. Palmans, *Chem. Soc. Rev*. 2012, 41, 6125-6137.

[4] C. A. Hunter and J. K. M. Sanders, *J. Am. Chem. Soc*. 1990, 112, 5525–5534.

[5] L. Brunsveld, H. Zhang, M. Glasbeek, J. A. J. M. Vekemans and E.W. Meijer, *J. Am. Chem. Soc*. 2000, 122, 6175–6182.

[6] S. Cantekin, T. F. A. de Greef and A. R. A. Palmans, *Chem. Soc. Rev.* 2012, 41, 6125.

[7] T. Wöhrle, I. Wurzbach, J. Kirres, A. Kostidou, N. Kapernaum, J. Litterscheidt, J. C. Haenle, P. Staffeld, A. Baro, F. Giesselmann and S. Laschat, *Chem. Rev*. 2016, 116, 1139–1241.

[8] Y. Matsunaga, N. Miyajima, Y. Nakayasu, S. Sakai and M. Yonenaga, *Bull. Chem. Soc. Jpn*. 1988, 61, 207–210.

[9] M. M. J. Smulders, M. M. L. Nieuwenhuizen, T. F. A. de Greef, P. van der Schoot, A. P. H. J. Schenning and E. W. Meijer, *Chem. Eur. J*. 2010, 16, 362–367;

[10] M. M. J. Smulders, A. P. H. J. Schenning and E. W. Meijer, *J. Am. Chem. Soc*. 2008, 130, 606–611.

[11] P. Besenius, J. L. M. Heynens, R. Straathof, M. M. L. Nieuwenhuizen, P. H. H. Bomans, E. Terreno, S. Aime, G. J. Strijkers, K. Nicolay and E. W. Meijer, *Contrast Media Mol. Imaging*, 2012, 7, 356-361.

[12] M. Gelinsky, R. Vogler and H. Vahrenkamp, *Inorg. Chem.* 2002, 41, 2560-2564.

[13] K. E. Broaders, S. J. Pastine, S. Grandhe and J. M. J. Fréchet, *Chem. Commun*. 2011, 47, 665-667.

[14] C. A. Jiménez, J. B. Belmar, L. Ortíz, P. Hidalgo, O. Fabelo, J. Pasán, and C. Ruiz-Pérez, *Cryst. Growth Des.* 2009, 9, 12, 4989.

[15] A. Paikar, A. Pramanik and D. Haldar, *RSC Adv.* 2015, 5, 31845.

[16] A. R. A. Palmans, J. A. J. M. Vekemans, E. E. Havinga and E. W. Meijer, *Angew. Chem. Int. Ed. Engl*. 1997, 36, 2648–2651.

[17] M. L. Bushey, A. Hwang, P. W. Stephens and C. Nuckolls, *J. Am. Chem. Soc*. 2001, 123, 8157–8158.

[18] P. J. M Stals, M. M. J. Smulders, R. Martín-Rapún, A. R. A. Palmans and E. W. Meijer, *Chem. Eur. J.* 2009, 15, 2071.

[19] C. Invernizzi, C. Dalvit, H. Stoeckli-Evans and R. Neier, *Eur. J. Org. Chem*. 2015, 5115–5127.

[20] K. K. Bejagam, G. Fiorin, M. L. Klein and S. Balasubramanian, *J. Phys. Chem. B* 2014, 118, 5218.

[21] I. A. W. Filot, A. R. A. Palmans, P. A. J. Hilbers, R. A. van Santen, E. A. Pidko and T. F. A. de Greef, *J. Phys. Chem. B* 2010, 114, 13667.

[22] C. Kulkarni, S. K. Reddy, S. J. George and S. Balasubramanian, *Chem. Phys. Lett.* 2011, 515, 226.

[23] A. Navarro, M. P. Fernández-Liencres, G. Garcia, J. M. Granadino-Roldán and M. Fernández-Gómez, *Phys. Chem. Chem. Phys.* 2015, 17, 605.

[24] M. Wegner, D. Dudenko, D. Sebastiani, A. R. A. Palmans, T. F. A. de Greef, R. Graf and H. W. Spiess, *Chem. Sci.* 2011, 2, 2040.

[25] S. I. Stupp and L. C. Palmer, *Chem. Mater*. 2014, 26, 507–518.

[26] R. R. Ernst, G. Bodenhausen and A. Wokaun, *Principles of Nuclear Magnetic Resonance in One and Two Dimensions*, International Series of Monographs on Chemistry, Clarendon Press, Oxford, 1987.

[27] T. D. W. Claridge, *High-resolution NMR techniques in organic chemistry*, Elsevier, Oxford, 2nd edn, 2009.

[28] D. Neuhaus and M. P. Williamson, *The nuclear Overhauser effect in structural and conformational analysis*, Wiley, New York, 2nd edn, 2000.

[29] A. A. Bothner-By, R. L. Stephens, J.-M. Lee, C. D. Warren and R. W. Jeanloz, *J. Am. Chem. Soc*., 1984, 106, 811–813.

[30] A. Bax and D. G. Davis, *J. Magn. Reson*., 1985, 63, 207–213.

[31] D. Appavoo, N. Raja, R. Deschenaux, B. Therrien and D. Carnevale, *Dalton Trans*., 2016, 45, 1410-1421.

[32] The *right-most term* in Equation (2) as shown in [31] applies only in the case of *n* = 2 and is therefore not of general validity.

[33] S. J. F. Vincent, C. Zwahlen, C. B. Post, J. W. Burgner and G. Bodenhausen, *Proc. Natl. Acad. Sci. U. S. A*., 1997, 94, 4383–4388.

[34] M. J. Duer, *Solid-State NMR Spectroscopy: Principles and Applications*, Blackwell Science, UK, 2002.

[35] E. R. Andrew, A. Bradbury and R. G. Eades, *Nature*, 1958, 182, 1659.

[36] I. Lowe, *Phys. Rev. Lett*., 1959, 22, 133.

[37] R. M. Orr, M. J. Duer and S. E. Ashbrook, *J. Magn. Reson*., 2005, 174, 301.

[38] R. M. Orr and M. J. Duer, *Solid State Nucl. Magn. Reson*., 2006, 30, 1.

[39]   C. Crockford, H. Geen and J. J. Titman, *Chem. Phys. Lett.*, 2001, 344, 367.

[40]   L. Shao, C. Crockford, H. Geen, G. Grasso and J. J. Titman, *J. Magn. Reson.*, 2004, 167, 75.

[41]   M. R. Mitchell, D. Carnevale, R. Orr, K. R. Whittle and S. E. Ashbrook, *J. Phys. Chem. C*, 2012, 116, 4273-4286.

[42]   D. Carnevale, S. E. Ashbrook and G. Bodenhausen, *RSC Adv.*, 2014, 4, 56248.

[43]   U. Haeberlen, *Advances in Magnetic Resonance*, Suppl. 1, J. S. Waugh Ed., Academic Press, New York, 1976.

[44]   R. G. Parr and W. Yang, *Density-Functional Theory of Atoms and Molecules*, Oxford Univ. Press, Oxford, 1989.

[45]   A. Bagno, F. Rastrelli and G. Saielli, *J. Phys. Chem. A*, 2003, 107, 9964–9973.

[46]   C. Bonhomme, C. Gervais, F. Babonneau, C. Coelho, F. Pourpoint, T. Azaïs, S. E. Ashbrook, J. M. Griffin, J. R. Yates, F. Mauri and C. J. Pickard, *Chem. Rev.*, 2012, 112, 5733–5779.

[47]   M. W. Stanford, F. R. Knight, K. S. Athukorala Arachchige, P. S. Camacho, S. E. Ashbrook, M. Bühl, A. M. Z. Slawin and J. D. Woollins, *Dalton Trans.*, 2014, 43, 6548–6560.

[48]   F. R. Knight, R. A. M. Randall, K. S. Athukorala Arachchige, L. Wakefield, J. M. Griffin, S. E. Ashbrook, M. Bühl, A. M. Z. Slawin and J. D. Woollins, *Inorg. Chem.*, 2012, 51, 11087–11097.

[49]   A. M. Jones, T. Lebl, S. Patterson, T. van Mourik, H. A. Früchtl, D. Philp, A. M. Z. Slawin and N. J. Westwood, *Tetrahedron*, 2009, 65, 563–578.

[50]   D. Carnevale, P. Wormald, B. Ameduri, R. Tayouo and S. E. Ashbrook, *Macromolecules*, 2009, 42, 5652–5659.

[51]   D. Carnevale, V. del Amo, D. Philp and S. E. Ashbrook, *Tetrahedron*, 2010, 66, 6238–6250.

[52]   M. Castro, V. R. Seymour, D. Carnevale, J. M. Griffin, S. E. Ashbrook, P. A. Wright, D. C. Apperley, J. E. Parker, S. P. Thompson, A. Fecant and N. Bats, *J. Phys. Chem. C*, 2010, 114, 12698–12710.

[53]   N. Salvi, J. Frey, D. Carnevale, M. Grätzel and G. Bodenhausen, *Dalton Trans.*, 2014, 43, 6389–6395.

[54]   D. Carnevale, A. J. Perez Linde, G. Bauer and G. Bodenhausen, *Chem. Phys. Lett.*, 2013, 580, 172–178.

[55]   A. J. Cohen, P. Mori-Sanchez and W. Yang, *Science*, 2008, 321, 792.

[56]   S. Grimme, J. Antony, T. Schwabe and C. Mück-Lichtenfeld, *Org. Biomol. Chem.*, 2007, 5, 741–758.

[57]   MOPAC2016, James J. P. Stewart, Stewart Computational Chemistry, Colorado Springs, CO, USA, HTTP://OpenMOPAC.net (2016).

[58]   A. D. Becke, *J. Chem. Phys.*, 1993, 98, 5648.

[59]   C. Lee, W. Yang and R. G. Parr, *Phys. Rev. B: Condens. Matter*, 1988, 37, 785.

[60]   S. Grimme, *J. Comput. Chem*., 2006, 27, 1787–1799.

[61]   Y. Minenkov, Å. Singstad, G. Occhipinti and V. R. Jensen, *Dalton Trans.* 2012, 41, 5526.

[62]   The mismatch produced by the B3LYP functional in the case of the NH irradiation when the pentameric structure is considered, has to have an affect also the other two measurements for the CH_2 and CH irradiations (red data in 4(a)). This is due to the fact that our three ROE experiments have been performed on a system of spins which may be seen as a closed and single one. In fact, when one of these spins is irradiated, a ROE enhancement is measured for the other two. Of these two enhancements, one is given an arbitrary and convenient value and the other is consequently determined. It is completely arbitrary which spin *X* in Equation (1) is chosen as reference, as it is only the ratio between enhancements I_X and I_B that is needed. By performing irradiation experiments on each of the three spins, we obtain three data sets that probe internuclear distances within this very single and closed three-spin system. In other words, in our case, an overestimation of one internuclear distance must result in a systematic overestimation of the other two. In fact, if an 'offset' distance is systematically subtracted from the red B3LYP data of 4(a), then one would obtain a profile of mismatches very similar to that produced by both B3LYP-D and B97D.

[63]   A. Rapp, I. Schnell, D. Sebastiani, S.P. Brown, V. Percec and H. W. Spiess, *J. Am. Chem. Soc.* 2003, 125, 13284.

[64]   T. Metzroth, A. Hoffmann, R. Martín-Rapún, M. M. J. Smulders, K. Pieterse, A. R. A. Palmans, J. A. J. M. Vekemans, E. W. Meijer, H. W. Spiess and J. Gauss, *Chem. Sci.* 2011, 2, 69.

[65]   S. P. Brown and H. W. Spiess, *Chem. Rev.* 2001, 101, 4125.

[66]   S. P. Brown, I. Schnell, J. D. Brand, K. Müller and H. W. Spiess, *J. Am*. *Chem. Soc.* 1999, 121, 6712.

[67]   S. V. Dvinskikh, J. Thaning, B. Stevensson, K. Jansson, S. Kumar, H. Zimmermann and A. Maliniak, *Phys. Rev. E*, 2006, 74, 021703.

[68]   B. Stevensson, A. Marini, H. Zimmermann and A. Maliniak, *J. Phys. Chem. B*, 2011, 115, 7561-7567.

[69]   Z. Tošner, R. Andersen, B. Stevensson, M. Edén, N.C. Nielsen and T. Vosegaard, *J. Magn. Reson*., 2014,246, 79.

[70]   M. J. Frisch, G. W. Trucks, H. B. Schlegel, G. E. Scuseria, M. A. Robb, J. R. Cheeseman, G. Scalmani, V. Barone, B. Mennucci, G. A. Petersson, H. Nakatsuji, M. Caricato, X. Li, H. P. Hratchian, A. F. Izmaylov, J. Bloino, G. Zheng, J. L. Sonnenberg, M. Hada, M. Ehara, K. Toyota, R. Fukuda, J. Hasegawa, M. Ishida, T. Nakajima, Y. Honda, O. Kitao, H. Nakai, T. Vreven, J. A. Montgomery Jr., J. E. Peralta, F. Ogliaro, M. Bearpark, J. J. Heyd, E. Brothers, K. N. Kudin, V. N. Staroverov, R. Kobayashi, J. Normand, K. Raghavachari, A. Rendell, J. C. Burant, S. S. Iyengar, J. Tomasi, M. Cossi, N. Rega, J. M. Millam, M. Klene, J. E. Knox, J. B. Cross, V. Bakken, C. Adamo, J. Jaramillo, R. Gomperts, R. E. Stratmann, O. Yazyev, A. J. Austin, R. Cammi, C. Pomelli, J. W. Ochterski, R. L. Martin, K. Morokuma, V. G. Zakrzewski, G. A. Voth, P. Salvador, J. J. Dannenberg, S. Dapprich, A. D. Daniels, Ö. Farkas, J. B. Foresman, J. V. Ortiz, J. Cioslowski and D. J. Fox, Gaussian 09, Revision A.01, Gaussian, Inc., Wallingford CT, 2009.

[71]   S. Sneddon, D. M. Dawson, C. J. Pickard and S. E. Ashbrook, *Phys. Chem. Chem. Phys*., 2014, 16, 2660-2673.

[72] J. Tomasi, B. Mennucci and R. Cammi, *Chem. Rev.*, 2005, 105, 2999-3093.

[73] D. Zeroka and H. F. Hameka, *J. Chem. Phys.*, 1966, 45, 300.

[74] R. Ditchfield, *J. Chem. Phys.*, 1972, 56, 5688.

Tables

Table 1   Calculated interplane dihedral angles (deg) across H-C-C-H and O=C-C-C-C=O nuclei, where the first two nuclei of each four defining the angle belong to the nth unit of the pentameric columnar assembly and the second two atoms belong to the nth+1 unit. These dihedral angles represent a measure of the twist experienced by the BTA units in the pentameric self-assembly around the column axis. The errors on the averaged angles are given by the standard deviation σ of all relevant values.

	Units	HCCH			OCCCCO			Average ± σ
B3LYP	1st-2nd	58.5	57.6	57.8	57.0	57.6	57.5	58.6 ± 1.0
	2nd-3rd	59.8	60.4	58.9	59.6	58.7	59.9	
	3rd-4th	59.2	59.3	58.7	59.3	59.5	59.2	
	4th-5th	57.4	57.3	57.4	58.3	58.5	58.3	
B3LYP-D	1st-2nd	65.5	66.0	65.9	66.4	66.2	66.3	62.8 ± 2.0
	2nd-3rd	61.9	62.1	61.9	60.5	62.7	62.0	
	3rd-4th	61.1	61.2	60.5	61.8	62.8	61.4	
	4th-5th	60.7	60.7	61.5	63.4	61.4	62.9	
B97D	1st-2nd	59.9	60.5	61.4	61.5	61.3	63.1	62.7 ± 2.4
	2nd-3rd	62.0	62.0	61.3	62.4	64.5	63.9	
	3rd-4th	61.1	60.7	60.7	59.9	60.1	62.2	
	4th-5th	64.8	65.7	67.6	65.0	67.6	66.4	

Table 2   Dihedral angles (deg) across H-<u>C</u>-<u>C</u>-<u>C</u>=<u>O</u> nuclei belonging to each BTA unit of a pentameric self-assembly as calculated with the B3LYP, B3LYP-D and B97D functionals. These dihedral angles measure the orientation of the amide functions in the self-assembly with respect to the aromatic cores. The errors on the averaged angles are given by the standard deviation σ of all relevant values.

	Unit	H<u>CCC</u>O			Unit average ± σ	Average ± σ
	1st	−30.7	−29.8	−33.5	−31.3 ± 1.9	
	2nd	−35.3	−37.7	−36.3	−36.4 ± 1.3	
B3LYP	3rd	−38.4	−38.3	−38.1	−38.3 ± 0.1	−34.4 ± 3.6
	4th	−36.1	−36.8	−36.9	−36.6 ± 0.4	
	5th	−29.5	−29.7	−29.3	−29.5 ± 0.2	
	1st	−29.2	−31.0	−26.1	−28.8 ± 2.5	
	2nd	−32.6	−30.0	−36.2	−32.9± 3.1	
B3LYP-D	3rd	−33.0	−33.4	−33.8	−33.4 ± 0.4	−28.6 ± 6.0
	4th	−29.9	−28.9	−30.7	−29.8 ± 0.9	
	5th	−18.9	−17.3	−17.9	−18.0 ± 0.8	
	1st	−35.2	−25.7	−26.8	−29.2 ± 5.2	
	2nd	−28.9	−32.8	−32.6	−31.4 ± 2.2	
B97D	3rd	−31.9	−30.2	−32.8	−31.7 ± 1.3	−25.9 ± 11.4
	4th	−25.3	−35.5	−27.5	−29.4 ± 5.4	
	5th	−17.9	−15.5	9.60	−7.9 ± 15.2	

Table 3   Chemical shift anisotropy Δ_{CS} and asymmetry η_{CS} parameters for the three relevant carbon sites as measured from 1D spectra and from the 2D CSA Amplification experiment.

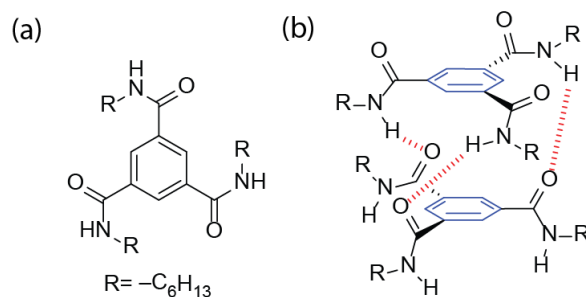|		1D CP MAS		2D CSA Amplification	
Site	δ_{iso} (ppm)	Δ_{CS} (ppm)	η_{CS}	Δ_{CS} (ppm)	η_{CS}
C=O	168.8	−85	0.76	−73 ± 4	0.85 ± 0.12
C	136.4	−109	0.21	−108 ± 6	0.60 ± 0.09
CH	126.2	−105	0.68	−107 ± 3	0.70 ± 0.09

Figures

Figure 1   (a) Structure of the *N,N',N''*-trihexylbenzene-1,3,5-tricarboxamide (BTA)
considered in this study. (b) Scheme depicting a dimeric columnar self-assembly
of BTA and highlighting the main interactions that drive the self-assembly, i.e.,
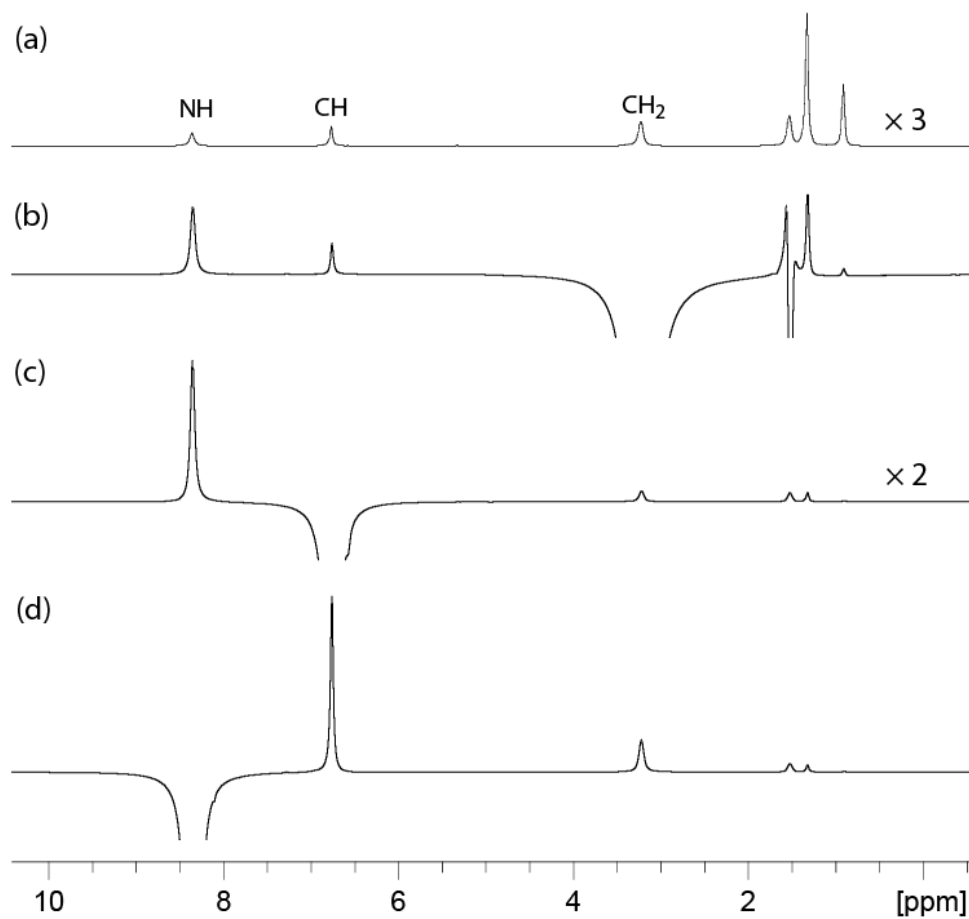hydrogen bonds, in red, and π-π stacking interactions between aromatic benzene
rings, in blue.

Columnar self-assembly of N,N',N''-trihexylbenzene-1,3,5-tricarboxamides investigated by means of NMR spectroscopy and computational methods in solution and solid state

30

Figure 2   (a) Proton NMR spectrum of a 177 mM solution of BTA in CD_2Cl_2 at 9.4 T (400 MHz). (b-d) ROE spectra on the same sample of (a) where the irradiated peak were the CH_2 at 3.24 ppm, the CH at 6.88 ppm and the NH at 8.22 ppm, respectively. The number of scans was 4 in (a) and 3072 in (b-d). A spin locking time of 5 ms was used for the ROE spectra of (b-d).
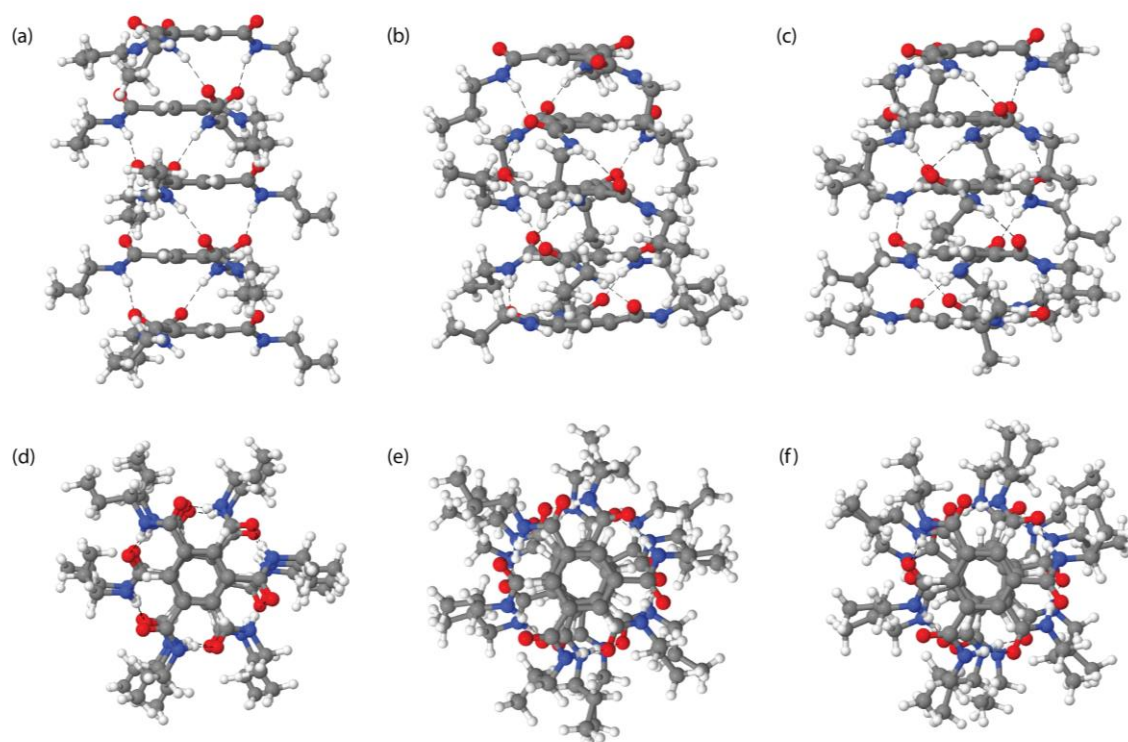
Figure 3   (a) Pentameric columnar structures of BTA as obtained with DFT methods at the B3LYP/6-31G(d,p) level of theory. (b,c) Structure analogous to that of (a) produced by the functionals B3LYP-D and B97D, respectively. (d-f) View down the helix column axis of the structure in (a-c). Hexyl aliphatic chains have been truncated to propyls to reduce computational times. Hydrogen, carbon, oxygen and nitrogen atoms are shown in white, grey, red and blue, respectively. Cartesian coordinates are given in the ESI.
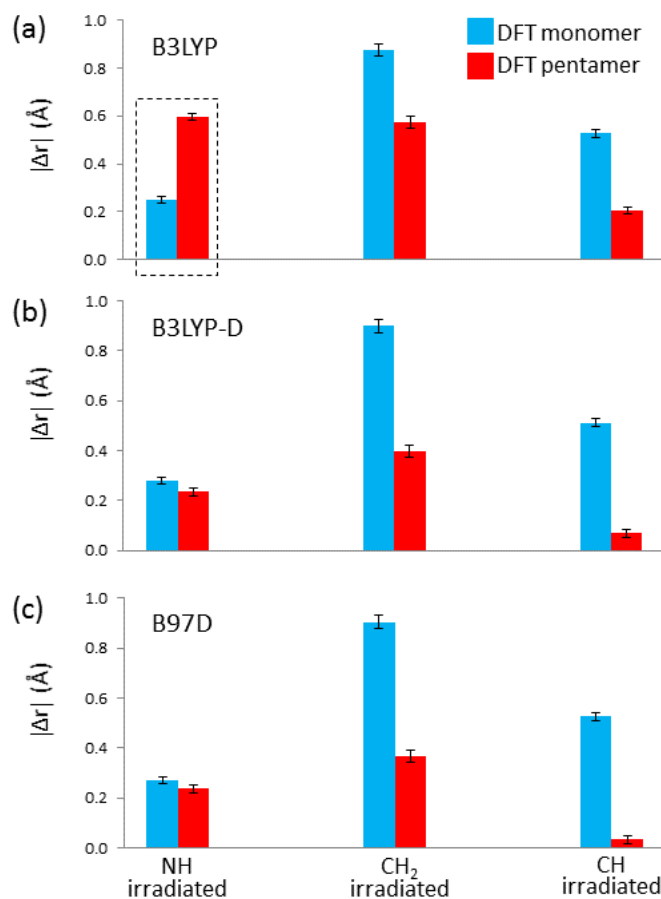
Figure 4   (a) Histogram of differences $|\Delta r|$ = $|r_{ROE} − r_{DFT}|$ between interatomic distances as calculated with B3LYP and those measured from the experiments of Figure 1. (b,c) Histograms analogous to that of (a) for distances taken from structures optimized with the B3LYP-D and B97D functionals. The error bars refer to the experimental data and were calculated with Equation (1) and (2) where the intensity of enhancement of the i-th spin was $I_i = \overline{I_i} \pm \sigma_i$, with $\overline{I_i}$ being the average intensity of five independent integrations of the i-th peak and σ_i being the standard deviation of the five integral values. Numerical values are given in Tables ESI1-3.
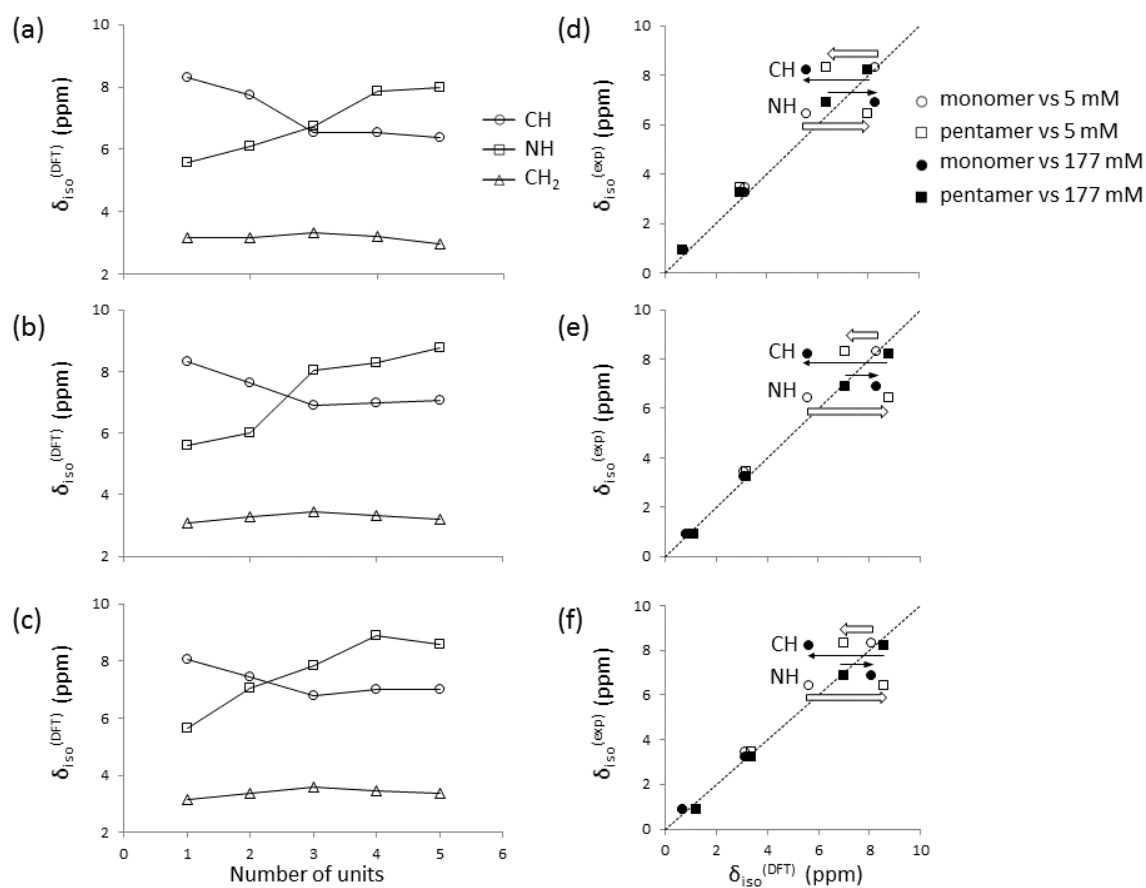
Figure 5   (a-c) Calculated variations of proton chemical shifts for the CH, NH and CH$_2$ sites as the columnar assembly is progressively increased from one to five units of BTA for B3LYP, B3LYP-D and B97D methods, respectively. (d-f) Correlation between calculated and experimental chemical shifts for B3LYP, B3LYP-D and B97D methods, respectively. Numerical values are given in Tables ESI4-7.
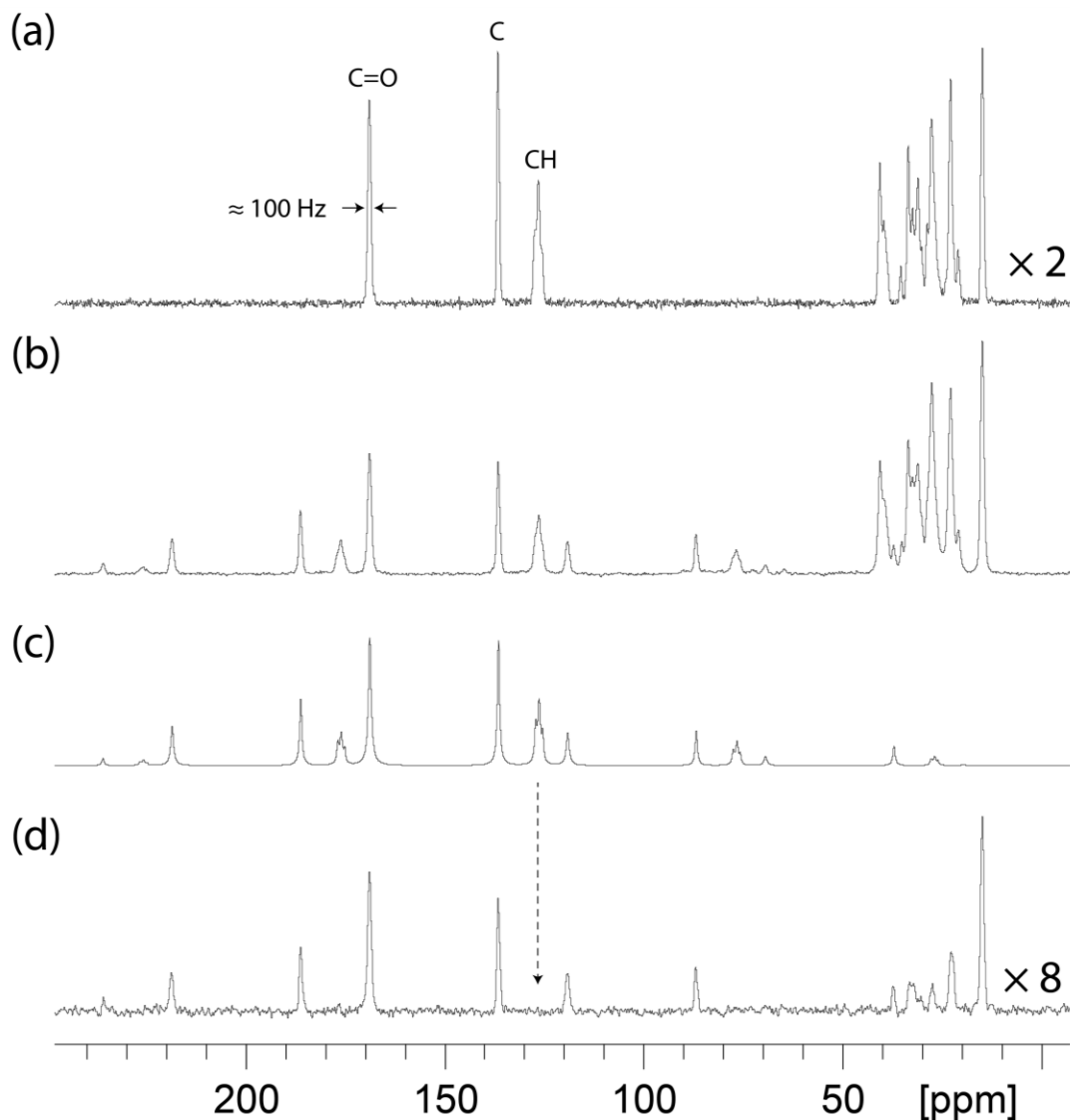
Columnar self-assembly of N,N',N''-trihexylbenzene-1,3,5-tricarboxamides investigated
by means of NMR spectroscopy and computational methods in solution and solid state

34

Figure 6   (a) ^{13}C CP MAS NMR spectra of a BTA powder in a 9.4 T magnet at a spinning rate v_{rot} = 20 kHz resulting from the averaging of 2800 scans and 2 Hz line broadening applied to the Free Induction Decay (FID). (b) Spectrum analogous to that of (a) at a spinning rate v_{rot} = 5 kHz and 20 Hz line broadening applied to the FID. (c) Numerical fit of the spectrum of (b) assuming one environment for the peak at 168.8 ppm, one environment for the peak at 136.4 ppm and three environments to take into account the shoulders of the peak at 126.2 ppm. The aliphatic region was not considered in the fit. (d) Dipolar dephasing spectrum of the same sample acquired at v_{rot} = 5 kHz and showing attenuation of the peaks associated to carbon sites bond to protons. 576 transients were averaged in this latter case, with 20 Hz line broadening applied to the FID.
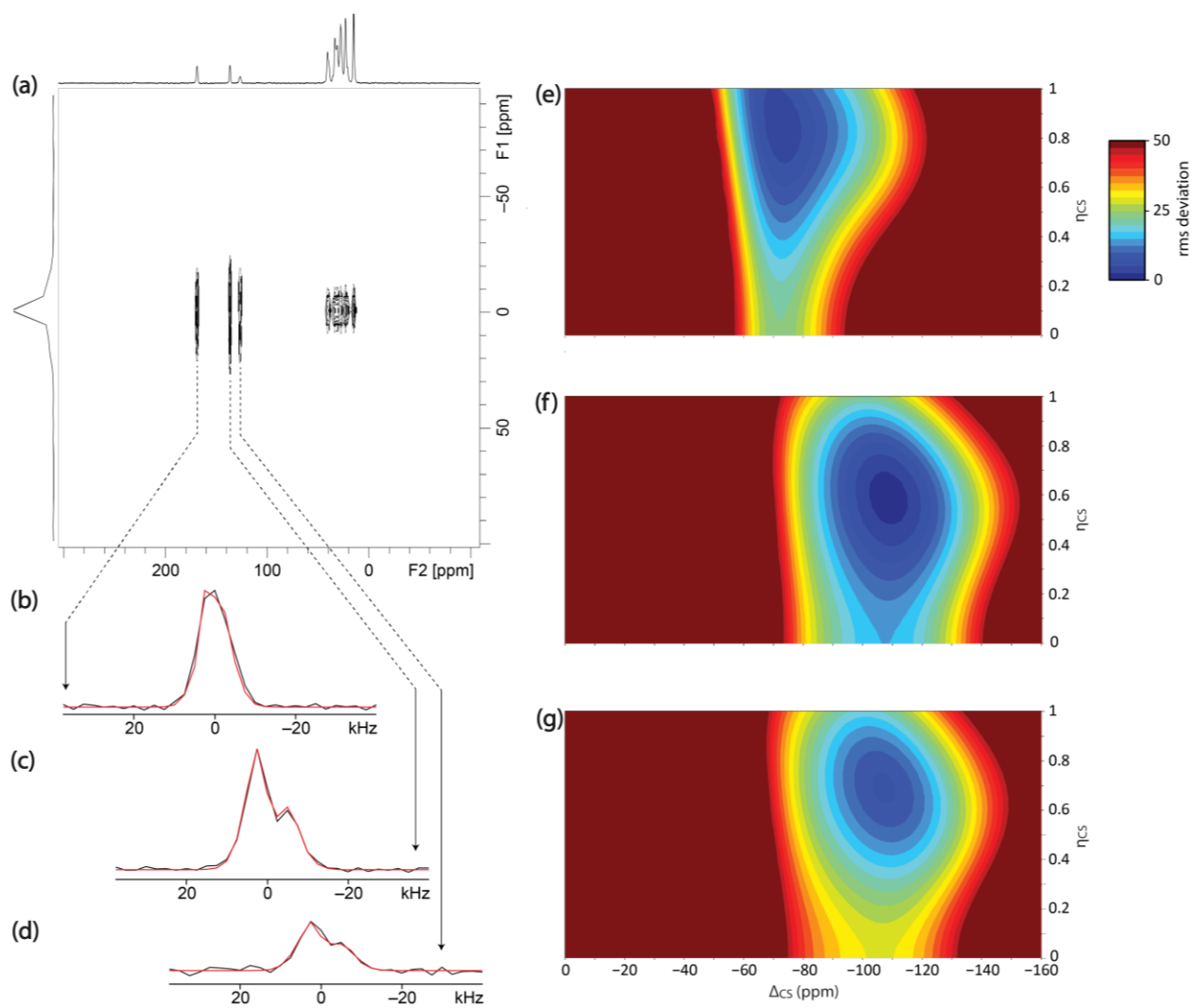
Figure 7   (a) ^{13}C CP CSA Amplification MAS NMR spectrum of a BTA powder recorded in a 9.4 T magnet at a spinning rate v_{rot} = 20 kHz. (b-d) Projections of the CO, C and CH sites, respectively, as extracted from the 2D spectrum of (a). Fits are shown in red, overlaid with the experimental data points, corresponding to spinning sideband envelopes as recorded at a fictitious spinning rate of 20/8 = 2.5 kHz. (e-f) 2D plots of the *rms* deviations of the fits of (b-d), respectively. Resolutions in the anisotropy Δ_{cs} and asymmetry η_{cs} dimensions were 100 Hz (1 ppm at 9.4 T) and 0.025, respectively, with intensity scale arbitrarily limited to 50.
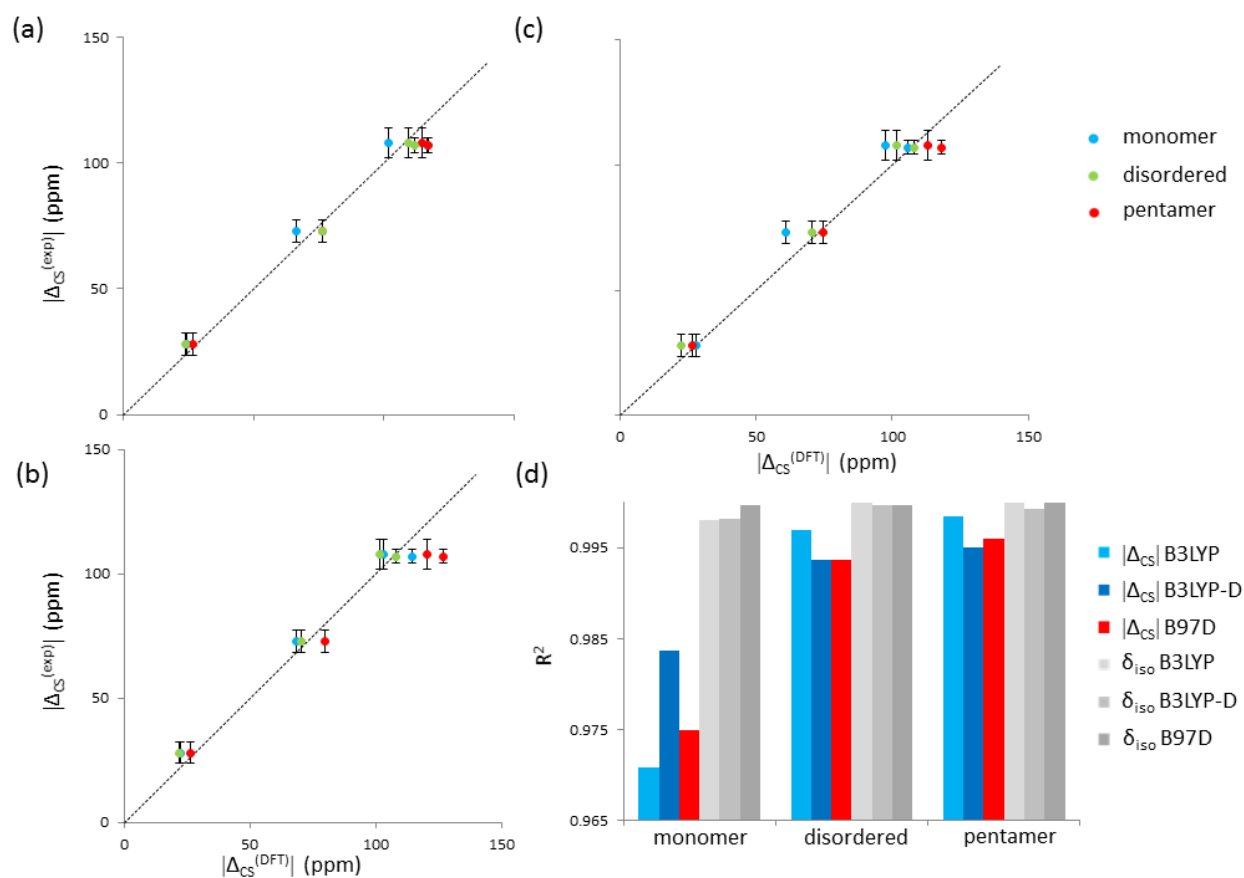
Figure 8   (a) Correlation between chemical shift anisotropies as calculated with the B3LYP functional for the considered structures and those as measured with the experiment of Fig. 7. (b,c) Correlations analogous to those of (a) for the computational data set as produced by the B3LYP-D and B97D functionals. (d) Histogram showing the correlation coefficients R^2 for anisotropy and isotropic shift of (a-c). Values are given in Tables ESI8-11.
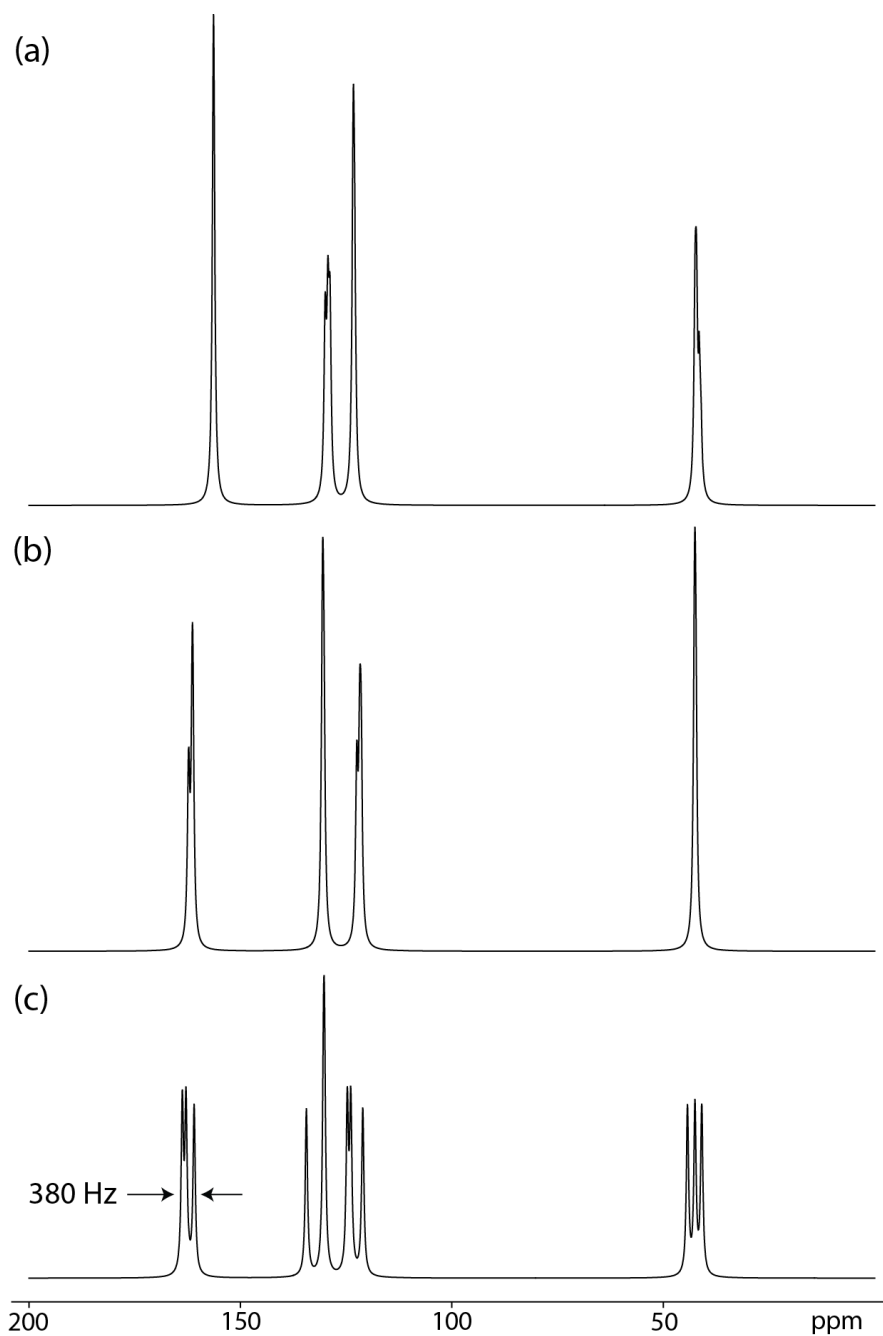
Figure 9   (a) Simulated ^{13}C NMR spectrum using the isotropic chemical shifts of all considered carbons in monomeric BTA. (b) Spectrum analogous to that of (a) using carbon chemical shift as calculated for a pentameric columnar assembly. (c) Carbon spectrum resulting from carbon shifts as calculated for the disordered arrangement of BTA unit of Fig. 9(c). The arrows highlight a FWHM of 380 Hz, given by the calculated spread of shifts of 280 Hz and a line broadening of 100 Hz, as used for all Lorentzian lineshapes.
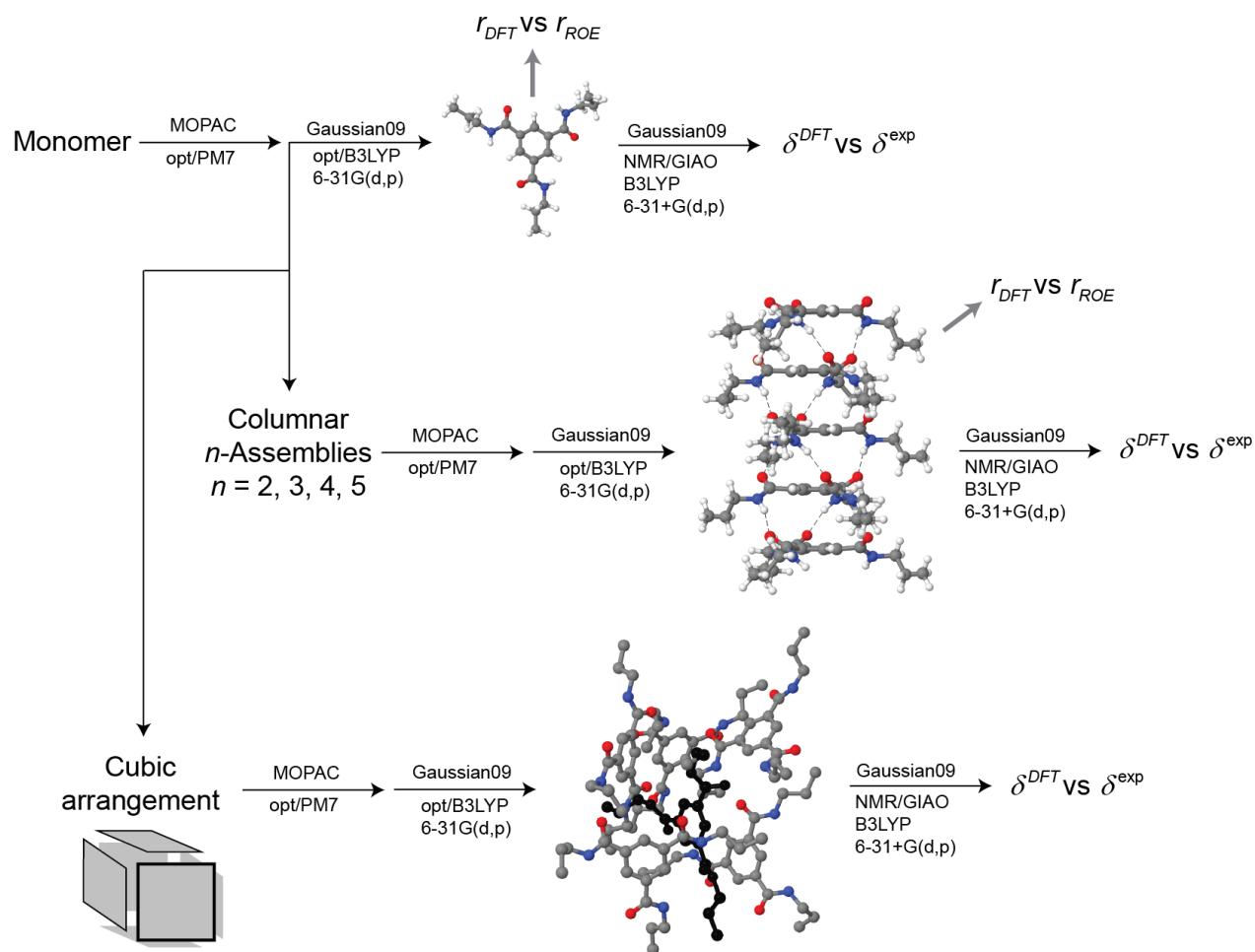
Figure 10   Scheme depicting the computational approach adopted in this study. All DFT steps have been also performed with the B3LYP-D and B97D functionals. Optimized structures were used to measure interatomic distances to be compared with those measured by ROE experiments and for the calculations of the full shielding tensors so as to compare isotropic and anisotropic parts of the interactions with those measured experimentally in both solution and solid state.